The electrochemical reduction of dioxygen and hydrogen peroxide by molecular copper catalysts

Langerman, M.

Chapter 4

Dioxygen reduction in acetonitrile: the influence of acid strength on the catalytic reaction

The pyridylalkylamine copper complex $[Cu(tmpa)(L)]^{2+}$ has previously been proposed to reduce dioxygen via a dinuclear resting state, based on experiments in organic aprotic solvents using chemical reductants. Conversely, a mononuclear reaction mechanism was observed under electrochemical conditions in a neutral aqueous solution. We have investigated the electrochemical oxygen and hydrogen peroxide reduction reaction catalysed by $[Cu(tmpa)(L)]^{2+}$ in acetonitrile, using several different acids over a range of pK_a. We demonstrate that strong acids lead to the loss of redox reversibility and to the destabilization of the copper complex under non-catalytic conditions. Under milder conditions, the electrochemical oxygen reduction reaction (ORR) was shown to proceed via a mononuclear catalytic intermediate, similar to what we have previously observed in water. However, in acetonitrile the catalytic rate constants of the ORR are dramatically lower by a factor 10^5, which is caused by the unfavourable equilibrium of formation of $[Cu^{II}(O_2^{\bullet-})(tmpa)]^+$ in acetonitrile. This results in higher catalytic rates for the reduction of hydrogen peroxide than for the ORR.

4.1.   Introduction

For the electrocatalytic oxygen reduction reaction (ORR) by $[Cu(tmpa)(L)]^{2+}$ (L = solvent molecule; abbreviated as Cu-tmpa) in aqueous solution it was shown in Chapter 2 that the formation and reduction of H_2O_2 play an important role in the catalytic mechanism.[1] Yet, the very high catalytic rates observed for these reactions and the abundance of protons in the aqueous environment preclude clear identification of reaction intermediates. The reaction of Cu-tmpa and other pyridylalkylamine copper complexes with O_2 in non-aqueous solutions has been studied intensively by Karlin and others.[2-7] Several intermediate species in the reaction between Cu^I complexes and O_2 have been identified.[8-10] This wealth of available knowledge concerning the nature of reaction intermediates and their reaction kinetics may help shed light on the catalytic pathway of the ORR by homogeneous electrocatalysts. Thus far however, such studies have not been performed on the electrocatalytic reduction of O_2 by Cu-tmpa or related copper complexes in organic solvents. The main focus in many publications on the subject of the ORR by these copper complexes has been on the O_2 reduction in acetone mediated by ferrocene (Fc) as a reducing agent, as opposed to electrocatalytic reduction.[11-15]   It   was   shown   that   the   dinuclear   peroxido   complex $[\{Cu^{II}(tmpa)\}_2(\mu\text{-}O_2)]^{2+}$ is formed as a resting state upon the addition of O_2 to the Cu^I-tmpa compound, and that from this resting state dioxygen reduction can take place after addition of a proton source. Whether this dinuclear peroxido complex is responsible for the catalysis is unclear. For a similar complex with a pivalamido functional group attached to one of the pyridine arms, $[Cu(PV\text{-}tmpa)(L)]^{2+}$, it was shown that a mononuclear Cu-OOH species is formed upon addition of acid to a solution containing the dinuclear species, from which the catalytic cycle proceeds.[14] Thus, this shows that O_2 bridging between two Cu centres is perhaps not essential for the breaking of the O–O bond. Similarly, the related complex $[Cu(tepa)]^{2+}$ (tepa = tris[2-(2-pyridyl)ethyl]-amine) does not form a dinuclear species at all in the presence of O_2 and ferrocene in acetone, but is able to perform the 2-electron reduction of O_2 to H_2O_2 upon addition of $HClO_4$.[15] The proposed catalytic mechanisms for the electrochemical ORR in water and the ORR in acetone using sacrificial reductants are shown in Scheme 4.1.

We have shown in Chapter 2 that mechanistic details are not necessarily transferable from one system to the other, either due to differences between chemical and electrochemical reduction, such as much faster electrochemical electron transfer, the nature of the solvent, or the acidity of the protons involved in the catalytic mechanism. Therefore, an important next step would be to study the electrocatalytic ORR by Cu-tmpa in non-aqueous solutions, where the precise specification of all catalytic species under resting conditions is known, to help bridge the gap in knowledge between our electrochemical studies in water and the stoichiometric studies by Karlin
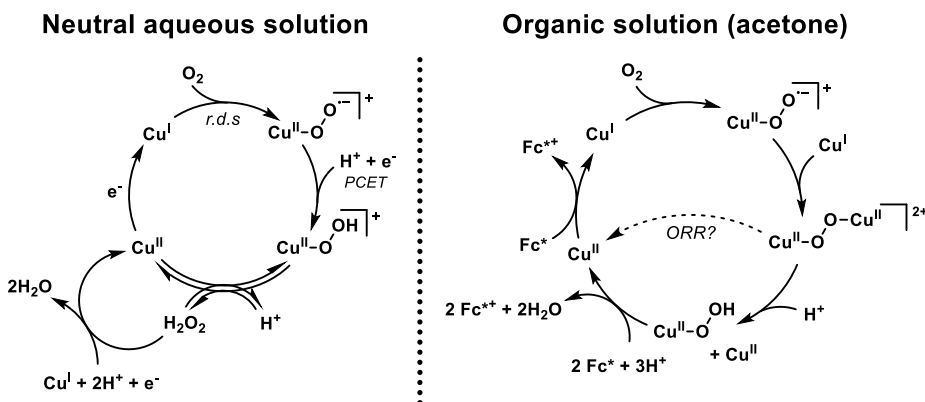
Scheme 4.1. Different catalytic mechanisms have been proposed for the reduction of O_2 by Cu-tmpa in neutral aqueous solution (electrocatalytic, Chapter 2),[1] and in acetone (ferrocene-mediated).[2, 11, 14] The tmpa ligand is excluded from the scheme for clarity.

et al. in organic solvents. Here, we report the electrochemical behaviour of Cu-tmpa in acetonitrile (MeCN), using several acids with a range of different pK_a values as proton donors. Additionally, the electrocatalytic performance of Cu-tmpa for the ORR and the hydrogen peroxide reduction reaction (HPRR) will be discussed, including the overpotential observed in a buffered electrolyte solution.

4.2. Results

4.2.1. Behaviour of Cu-tmpa in an MeCN electrolyte solution in the absence of acid

The redox behaviour of Cu-tmpa in an acetonitrile solution containing the supporting electrolyte NBu_4PF_6 (100 mM) was investigated in the absence of acids. Cyclic voltammograms (CVs) of Cu-tmpa in this solution were recorded using a Glassy Carbon (GC) working electrode (A = 0.0707 cm^2). When the solution is saturated with argon, a well-defined reversible Cu$^{II/I}$ redox couple is observed at $E_{1/2}$ = −0.41 mV vs. Fc$^+$/Fc with a peak-to-peak separation (ΔE_p) of 59 mV, shown in Figure 4.1a. This corresponds well to the previously reported half-wave potential for this complex in acetonitrile.[16] Upon saturation of the solution with 1 atm O_2, the initial reduction of Cu^{II} to Cu^I is still observed (Figure 4.1b). However, an additional reduction takes place when the applied potential is lower than −0.80 V. At the same time, the oxidative current associated with the oxidation of Cu^I to Cu^{II} is significantly lower than the same oxidative peak measured in the presence of 1 atm argon. Subsequent CV cycles in the same potential window (up to −1.1 V) also show a decrease of the Cu$^{II/I}$ reduction peak and an increase in of the ΔE_p from 56 mV in the first scan to 88 mV (Figure 4.1c). The oxidation at −0.35 V reappears
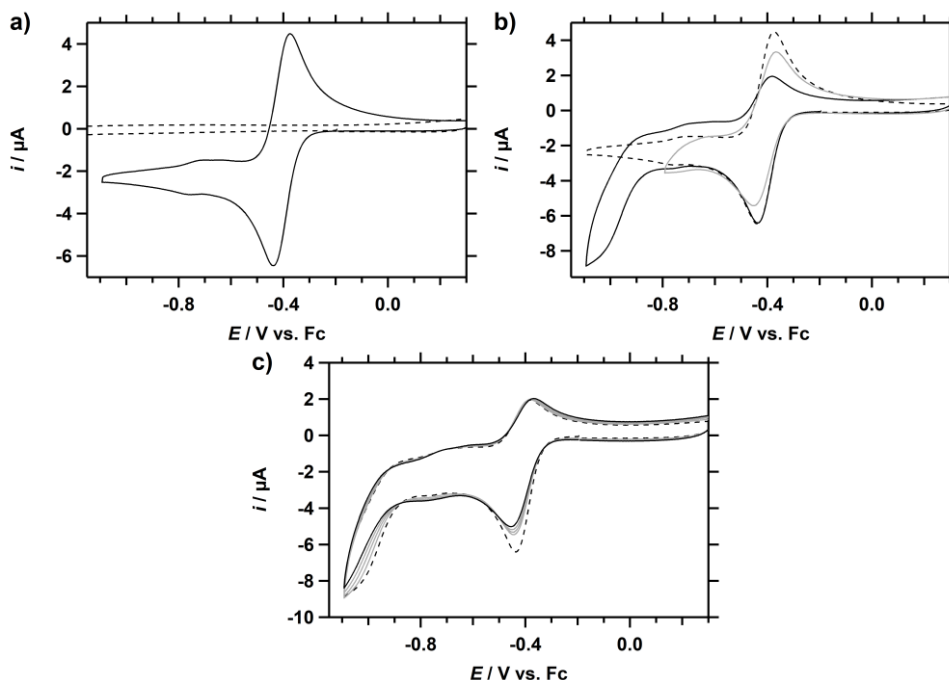
Figure 4.1. a) Cyclic voltammogram of Cu-tmpa (0.3 mM) in the absence of acid, including GC blank measurement (dashed), under 1 atm Ar. **b)** CVs of Cu-tmpa in the presence of 1 atm O_2 with varying potential windows. The redox couple in the presence of Ar is shown for comparison (dashed). **c)** CVs showing the redox behaviour in the presence of oxygen over 5 cycles; first scan (dashed trace) and last scan (solid trace). Conditions: NBu_4PF_6 (100 mM) in MeCN, 100 mV s^{-1}, 293 K.

when this measurement is repeated while limiting the lower limit of the potential window to −0.75 V (Figure 4.1b, grey trace). However, the ΔE_p remains at 88 mV and is stable over several scans.

4.2.2. On the topic of equilibrium potentials in non-aqueous solutions and homoconjugation of acids and conjugate bases

Much research has been performed on electrocatalytic reactions for small molecule conversion catalysed by transition metal complexes in non-aqueous electrolyte solutions, particularly MeCN and DMF, often for solubility reasons.[17-20] However, comparing the catalytic performance of different molecular electrocatalysts in different non-aqueous media using a range of different proton sources may pose a significant challenge. Thermodynamics of the catalytic reactions of interest vary wildly with differing conditions and are more challenging to probe than in aqueous solutions, where reactions can more easily be referenced to the H_2/H^+ couple, regardless of different acids, bases, or supporting electrolytes being used. To be able to determine

Table 4.1. Acid strength (pK_a) and homoconjugation formation constants (K_f) in MeCN of the acids used in this work.

Acid	pK_a	log(K_f)
HOAc	23.5 [26-27]	3.9 [27]
HNEt$_3^+$	18.8 [21]	n/a
HTFA	12.7 [26-27]	3.9 [27]
HDMF$^+$	6.1 [27]	1.6 [17]

the overpotential of the ORR in organic media, the equilibrium potential of the reaction has to be known for the given conditions. Recent work by Roberts and Bullock,[21] and Pegis, Appel and Mayer[22] has been key in providing a reliable method for determination of the equilibrium potential of the HER and in determining the standard potential of O_2/H_2O in MeCN and DMF, thus enabling more reliable and meaningful comparisons of the performance of catalysts towards the ORR.

However, the standard potentials for the catalytic reactions only apply when both the acid (HA or HB$^+$) and its base (A$^-$ or B) are present in the solution in equal amounts, as different ratios can cause significant shifts in the equilibrium potential of the studied reactions. This is especially relevant as there will be a significant decrease in [HA] and concurrent increase in [A$^-$] during the catalytic reaction, resulting in shift of the equilibrium potential as the catalytic reaction progresses. This requires the use of a buffered electrolyte for the determination of the overpotential, with equal concentrations of HA and A$^-$. One complicating factor connected to the use of such a buffered electrolyte solution is the occurrence of homoconjugation. Homoconjugation occurs when the base A$^-$ (or B) reacts with the acid HA (or HB$^+$), resulting in the formation of the conjugate species HA$_2^-$ (or HB$_2^+$). Thus, upon homoconjugation of the acid and the conjugate base, the effective concentration of available protons in the form of free HA is reduced. However, it does not affect the equilibrium potential, as the ratio of available [HA] to [A$^-$] does not change. The extend of this effect is dependent on the homoconjugation constant (K_f), which varies with different acids. The K_f values of the acids relevant to this work are shown in Table 4.1. It has been reported that triethylamine does not undergo homoconjugation.[23-25]

4.2.3. Stability and electrochemical behaviour of Cu-tmpa in the presence of different organic acids

To study the electrochemical activity of Cu-tmpa in acetonitrile, several different organic acids were used, namely triethylammonium (HNEt$_3^+$), acetic acid (HOAc), trifluoroacetic acid (HTFA), and dimethylformamidium (HDMF$^+$). These acids find
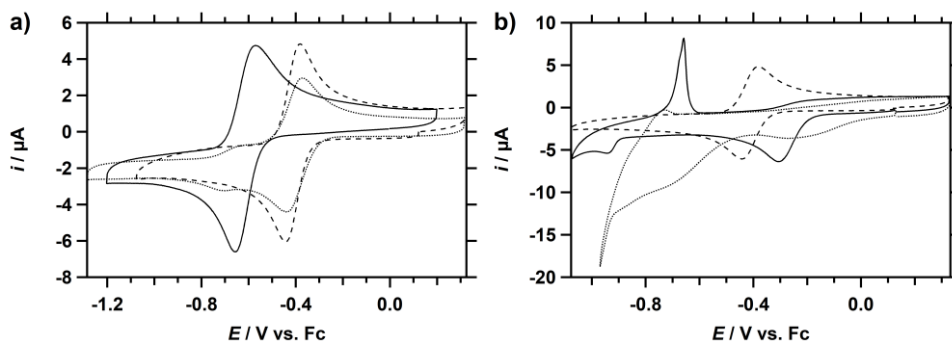
Figure 4.2. CVs of Cu-tmpa (0.3 mM) in a solution with **(a)** 50 mM HNEt₃PF₆ (solid) and 20 mM HOAc (dotted), and **(b)** 20 mM (HDMF)OTf (solid) and 20 mM TFA (dotted), under 1 atm Ar. For reference, a CV of the complex in absence of acid (dashed trace) is shown in both. Conditions: NBu₄PF₆ (100 mM) in MeCN, 100 mV s⁻¹, 293 K.

common use in homogeneous electrocatalysis as proton sources for HER and ORR and were chosen for their range of pK_a values in MeCN, as shown in Table 4.1. As the strength of the aforementioned acids span a wide range of pK_a, from very strong acid (HDMF)OTf to the very weakly acidic HNEt₃PF₆, the stability of Cu-tmpa in the presence of the selected acids was studied using both cyclic voltammetry and UV-vis absorption measurements (see Appendix C.9). Unless otherwise stated, all electrochemical measurements were performed in MeCN containing NBu₄PF₆ (0.1 M) as supporting electrolyte and the potential is reported versus the Fc⁺/Fc redox couple.

The CV of Cu-tmpa in 50 mM HNEt₃PF₆ saturated with 1 atm argon showed a reversible redox couple at −0.61 V (Figure 4.2). In an electrolyte solution containing HOAc (20 mM) a reversible redox couple is observed at −0.40 V, which is very close to the $E_{1/2}$ of the complex in the absence of acid. In the presence of either of these acids, the CV was shown to be very stable over multiple cycles. However, electrochemical stability was not observed in solutions containing HTFA or HDMF⁺. In the presence of HTFA, only the reduction of Cu^{II} to Cu^{I} is observed at −0.30 V, but the associated oxidation peak is absent. Scanning below −0.9 V reveals a small reduction event, while a sharp oxidative stripping peak appears on the forward scan of the CV. This behaviour is consistent with the deposition of metallic Cu⁰ on the electrode surface. With (HDMF)OTf the voltammogram is even less-defined, showing a broad first reduction starting below 0 V, followed by second broad reduction event below −0.5 V. Below $E =$ −0.9 V a sharp reduction is observed, which is indicative of proton reduction.

Although the voltammograms of the full potential window are shown in Figure 4.2, limiting the potential windows of the measurements to −0.5 V did not lead to the re-appearance of the Cu$^{II/I}$ oxidation peak, whether in a solution containing HTFA or (HDMF)OTf. Considering this lack of reversible redox couple, or as is the case with

62

(HDMF)OTf, the lack of clearly defined reduction and oxidation events that could be assigned to Cu-tmpa even under non-catalytic conditions, use of these acids was not further studied. In water, it was found that below pH 4 the stability of Cu-tmpa decreased, thought to be due to demetallation of a Cu^{II}-tmpa or Cu^{I}-tmpa complex, while the complex is stable under strongly alkaline conditions.[26] Protonation of the pyridine moieties at low pH is a likely cause for the observed instability of Cu-tmpa, both in water and organic solvents.

4.2.4. Comparison of catalytic activity between unbuffered and buffered acid conditions

4.2.4.1. *Acetic acid*

The redox and catalytic behaviour of Cu-tmpa was investigated by performing cyclic voltammetry measurements in a NBu_4PF_6 electrolyte solution containing HOAc or a buffered HOAc/OAc⁻ acid-conjugate base mixture, using a glassy carbon electrode. The resulting CVs are shown in Figure 4.3a. The $Cu^{II/I}$ redox couple with $E_{1/2}$ = −0.40 V has a ΔE_p of 66 mV in the electrolyte solution containing 20 mM HOAc saturated with 1 atm argon. Additionally, a small redox event is visible at −0.68 V. In the solution containing the acid-conjugate base pair HOAc/OAc⁻ (each 20 mM), the redox couple is shifted to a more negative potential, with $E_{1/2}$ = −0.73 V and a larger ΔE_p of 78 mV. However, only a single redox couple is observed under these conditions as opposed to the two distinct redox couples observed in HOAc. Coordination of acetate to Cu^{II} is responsible for the shift of the redox couple to a more negative couple, with the increased electron density resulting in a complex that is harder to reduce. Acetate coordination was also confirmed by UV-vis measurements of the absorption of Cu-tmpa in the presence of
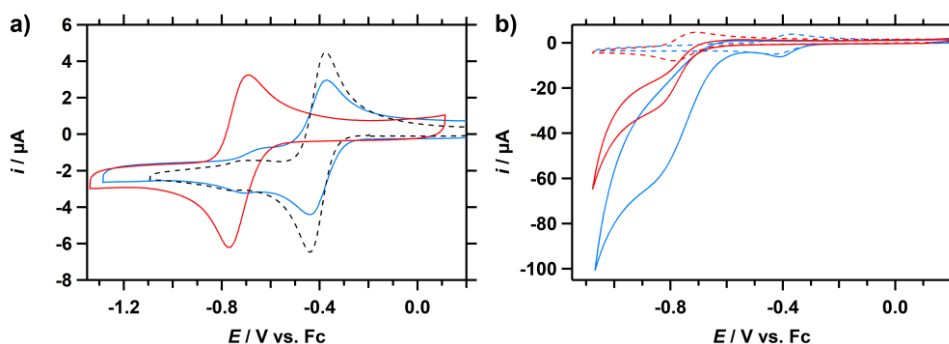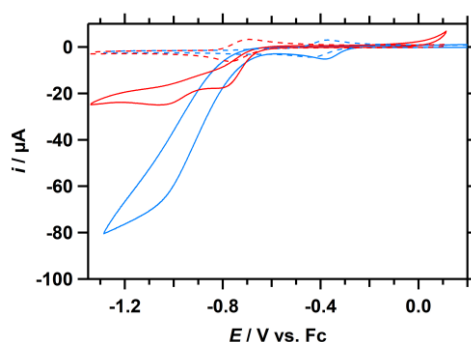

Figure 4.3. CV of Cu-tmpa (0.3 mM) under 1 atm Ar **(a)** and under 1 atm O₂ **(b)**, in the presence of 20 mM HOAc (blue) or 20 mM HOAc/OAc⁻ (each 20 mM; red). For reference, a CV of the complex in absence of acid under 1 atm Ar (dashed trace) is shown on the left. Conditions: NBu_4PF_6 (100 mM) in MeCN, 100 mV s⁻¹, 293 K.

HOAc/OAc⁻ (20 mM), based on the appearance of a sharp LMCT absorption peak around 300 nm and a blueshift of the d-d band, as can be seen in Figure C.12c (Appendix C.9).

Cu-tmpa shows very different catalytic characteristics under both conditions. When the solutions are saturated with O_2 a catalytic wave is observed in both cases (Figure 4.3b), however a lower catalytic current is observed for the buffered system. This is unsurprising, as homoconjugation lowers the amount of free acid in the solution compared to the situation where no conjugated base is present. With HOAc, the reduction from Cu^{II} to Cu^{I} is still distinctly visible, and the onset potential of the catalytic reaction is 220 mV below the peak reduction potential (E_{pc}) of −0.44 V in the absence of oxygen. Here, the catalytic onset potential is defined as the potential where the current is 1 µA higher than the current in the absence of the substrate. In the solution containing the acid-conjugate base pair, the reduction of Cu^{II} and the onset of catalysis overlap, and the catalytic half-wave potential ($E_{cat/2}$) of −0.77 V coincides closely with E_{pc} (−0.77 V). This is more easily visualized after performing a background correction of significant GC activity towards the ORR under these conditions. The resulting linear sweep voltammograms (LSVs) are show in Figure C.4 (Appendix C.3). The background corrected LSVs show a peak catalytic current (i_{cat}) of 56 µA in the solution containing HOAc, while the i_{cat} in the buffered solution is almost halved to 29 µA.

To get more insight into the catalytic pathway and the product that is formed, the reduction of H_2O_2 by Cu-tmpa was investigated. One key difference between the conditions in which the ORR and HPRR were performed is the presence of 30 mM of H_2O during the HPRR, as H_2O_2 was added in the form of a 30% solution in water. CVs of the complex in both unbuffered and buffered electrolyte solution are shown in Figure 4.4. As was the case for the ORR, the onset of H_2O_2 reduction in the presence of HOAc
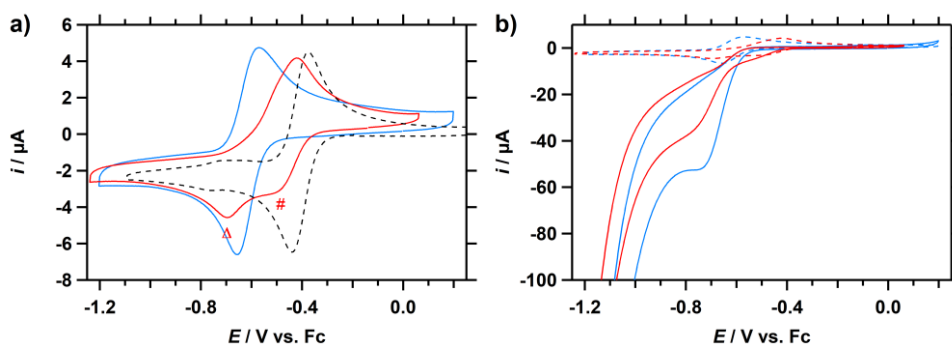

Figure 4.4. CV of Cu-tmpa (0.3 mM) under 1 atm Ar (dotted lines) and with 8.1 mM H_2O_2 under 1 atm Ar (solid lines), in the presence of 20 mM HOAc (blue) or HOAc/OAc⁻ (each 20 mM; red). Conditions: NBu₄PF₆ (100 mM) in MeCN, [H_2O] = 30 mM, 100 mV s⁻¹, 293 K.

only starts after the complex has been reduced to Cu^I. However, the onset potential of the HPPR is shifted by −100 mV versus the onset of the ORR. For the solution containing HOAc a single catalytic wave is observed, while for the buffered system a double S-shaped catalytic curve is visible with a much lower current, which again can be explained by a lowered availability of acidic protons compared to the electrolyte solution containing only HOAc, due to homoconjugation. However, the previously mentioned coordination of acetate may have an even greater influence on the HPRR in the buffered acetate system, resulting in a reduction of the catalytic activity compared to the unbuffered system.

4.2.4.2. *Triethylammonium*

Similarly, the use of protonated triethylamine as the proton donor for the ORR was investigated. Cyclic voltammograms were recorded in a NBu$_4$PF$_6$ electrolyte solution containing HNEt$_3^+$ (in the form of HNEt$_3$PF$_6$) or a buffered HNEt$_3^+$/NEt$_3$ acid-conjugate base mixture and are shown in Figure 4.5. In the presence of argon, the $E_{1/2}$ of the Cu-tmpa redox couple in the solution containing HNEt$_3^+$ is −0.61 V. Seemingly, Cu-tmpa has a well-defined single redox couple, although the somewhat large ΔE_p of 88 mV indicates a degree of irreversibility. On the other hand, in the solution containing the HNEt$_3^+$/NEt$_3$ acid-conjugate base pair, two distinct reductions are observed. One has a cathodic peak potential (E_{pc}) centred at −0.50 V (marked by #) and the second at −0.70 V (marked by Δ). These are paired with a broadened oxidation wave, which is caused by two overlapping redox couples. This is more evident when looking at a differential-pulse voltammogram (DPV) measured in the same solution (Figure C.3, Appendix C.2). In the DPV, a smaller oxidative peak is visible at a more negative potential, shifted by −0.20 V from the main oxidative peak. This is the same difference in potential as observed for
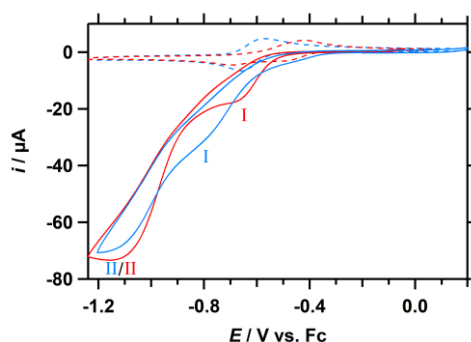

Figure 4.5. CVs of Cu-tmpa (0.3 mM) under 1 atm Ar **(a)** and under 1 atm O$_2$ **(b)**, in the presence of 50 mM HNEt$_3$PF$_6$ (blue) or HNEt$_3$PF$_6$/NEt$_3$ (each 50 mM; red). For reference, a CV of the complex in absence of acid under 1 atm Ar (dashed trace) is shown on in **(a)**. Conditions: NBu$_4$PF$_6$ (100 mM) in MeCN, 100 mV s^{-1}, 293 K.

the E_{pc} of the two reductive peaks. The $E_{1/2}$ of the main redox event is −0.462 V and has a ΔE_p of 81 mV. In the UV-vis absorption spectra, only a small 25 nm blueshift is observed for the d-d transition upon addition of $HNEt_3^+$ or $HNEt_3^+/NEt_3$ which could be indicating protonation of one of the coordinated nitrogen atoms of the tmpa ligand (see Figure C.12e/g, Appendix C.9). The behaviour of Cu-tmpa under these conditions is opposite to what was observed in presence of HOAc and HOAc/OAc⁻, where the redox couple was shifted to more negative potentials in the buffered electrolyte solution due to the presence of acetate, while no shift was observed in the solution with only HOAc. In section 4.2.6 we show that the redox potential in the presence of $HNEt_3^+$ is both dependent on acid concentration and time, showing that the behaviour of Cu-tmpa under these conditions is far from straightforward.

In the presence of 1 atm O_2, a catalytic response is observed in CV for both buffered and unbuffered electrolyte solutions containing 0.3 mM Cu-tmpa (Figure 4.5b). The catalytic onset in the unbuffered solution (−0.56 V) coincides with the redox potential of Cu-tmpa under argon. In the buffered solution the catalytic onset coincides with the previously discussed second redox event at −0.70 V (Figure 4.5a; Δ) that is observed in the same buffered solution under argon. As was observed with HOAc, Cu-tmpa shows a higher maximum current and a somewhat earlier onset in the unbuffered electrolyte solution, compared to that observed in the buffered electrolyte solution. The background corrected LSVs show an i_{cat} of 53 µA in the solution containing $HNEt_3^+$ (Figure C.4a), while the i_{cat} in the buffered $HNEt_3^+/NEt_3$ electrolyte solution is about a third lower at 35 µA (Figure C.4b).

The CVs of the catalytic response upon the addition of H_2O_2 to the electrolyte solutions containing 0.3 mM Cu-tmpa are shown in Figure 4.6. While similar peak catalytic currents are reached for both buffered and unbuffered solutions, some

Figure 4.6. CVs of Cu-tmpa under 1 atm Ar (dashed lines) and with 8.1 mM H_2O_2 under 1 atm Ar (solid lines), in the presence of 50 mM $HNEt_3PF_6$ (blue) or $HNEt_3PF_6/NEt_3$ (each 50 mM; red). Conditions: NBu_4PF_6 (100 mM) in MeCN, $[H_2O]$ = 30 mM, 100 mV s⁻¹, 293 K.

Table 4.2. Overview of the electrochemical properties of Cu-tmpa and its catalytic activity toward the ORR under different conditions.

	E_{pc} (V)	$E_{1/2}$ (V)	ΔE_p (mV)	$E_{onset, ORR}$	$E_{cat/2}$	i_{cat} (μA)
No acid	−0.44	−0.41	59	-	-	-
HNEt$_3$PF$_6$	−0.66	−0.61	88	−0.56	−0.65	53
HNEt$_3$PF$_6$/NEt$_3$	−0.50[a], −0.70[b]	−0.46	81	−0.52	−0.68	35
HOAc	−0.44	−0.40	66	−0.56	−0.73	56
HOAc/NBu$_4$OAc	−0.77	−0.73	78	−0.70	−0.77	29

[a] E_{pc} of the first reduction. [b] E_{pc} of the second reduction. E_{onset} is defined as the potential where the catalytic current i_{cat} is 1 μA higher than i_p under argon. Potential V vs. Fc$^+$/Fc

Table 4.3. Overview of the electrochemical properties of Cu-tmpa related to the catalytic reduction of H$_2$O$_2$ under different conditions.

	$E_{onset, HPRR}$	$E_{cat/2}$	i_{cat} (μA)
HNEt$_3$PF$_6$	−0.35	−0.59	40[a], 71
HNEt$_3$PF$_6$/NEt$_3$	−0.56	−0.60	19[b], 72
HOAc	−0.66	−0.88	77
HOAc/OAcNBu$_4$	−0.68	−0.72	18[a], 25

[a] catalytic current measured at −0.80 V. [b] Catalytic current measured at −0.75 V. E_{onset} is defined as the potential where current i_{cat} is 1 μA higher than i_p under argon.

differences can be observed. In both cases, the catalytic wave seems to consist of two different waves (I and II), but in the buffered solution the initial "peak" current (I) is reached at a higher potential and lower current, while for the unbuffered system a higher current is reached and more overlap between the first (I) and second (II) wave is observed, which precludes the formation of a current plateau for the first wave.

The electrochemical properties of Cu-tmpa in the presence of argon, O$_2$, and H$_2$O$_2$ for the different acid and acid-conjugate base systems, with equal concentrations of HA (or HB$^+$) and A$^-$ (or B), have been summarized in Table 4.2 and Table 4.3.

4.2.5.   OCP values for the determination of H$_2$/H$^+$ and the overpotential for the ORR in non-aqueous solutions

After it was established that of the four acids that were investigated only HNEt$_3^+$ and HOAc are viable acids for use in combination with Cu-tmpa under electrochemical conditions, the open-circuit potentials (OCPs) for these acidic solutions and buffered 1:1 acid-conjugate base solutions were determined. The OCP can be used as a direct measure of the equilibrium potential of the H$^+$/H$_2$ couple in organic solvent, which is especially useful in solvents where no robust pK_a scale is available and the standard

potential of the H$^+$/H$_2$ is not known.[21] In combination with the catalytic half-wave potential, the OCP can be used to determine overpotential and compare them with results obtained in different media.

The OCPs were measured using a platinum wire and averaged over a 60 second window in a 100 mM NBu$_4$PF$_6$ electrolyte solution saturated with H$_2$, containing the desired acid or acid-conjugate base mixture, and referenced versus Fc$^+$/Fc. The resulting OCP values are summarized in Table 4.4. Buffering of the HNEt$_3^+$ solution resulted in the largest OCP shift of −297 mV, while buffering of the HOAc containing solution resulted in a positive shift of 162 mV. To determine the effect of water in the acetonitrile solutions on the OCP, the OCP values were also determined for the same solutions containing 0.10 M H$_2$O. Adding water to acetonitrile solutions containing either only the acid or a 1:1 acid-conjugate base mixture does not have a large effect on the OCP, at most only shifting the potential by +29 mV in the case of the 1:1 HOAc/OAc$^-$ mixture. This also indicates that the in-situ generation of conjugate base during the electrocatalytic reaction will have a larger effect on local potential and pH than the generation of water during the same reaction.

To validate the experimental setup and the method that was used to determine the OCP, the values for the buffered HNEt$_3^+$/NEt$_3$ system were compared to the OCP values of HNEt$_3^+$ (used as a BF$_4^-$ salt) in MeCN as reported in the literature,[21] which is in agreement with the OCP value reported in Table 4.4. For HOAc/OAc$^-$ an OCP value of −1.207 V was measured, which would correspond to a standard reduction potential of H$^+$ (E_{H+}^0) of 0.159 V vs. Fc$^+$/Fc, after applying the Nernst equation on the measured OCP potential (Eq. 4.1). This is far removed from the previously established E_{H+}^0 in MeCN (0.028 V vs. Fc$^+$/Fc)[21], which indicates that the conditions during our OCP measurements for HOAc/OAc$^-$ were not sufficiently controlled to obtain accurate values for the OCP.

$$E_{H+}^0 = E_{OCP} + \frac{RT}{F}\ln(K_a) \qquad (4.1)$$

$$\eta = E_{OCP} - E_{cat/2} + (E_{O_2}^0 - E_{H+}^0) \qquad (4.2)$$

$$\eta = (E_{O_2}^0 - 0.0592pK_a) - E_{cat/2} \qquad (4.3)$$

Two different methods were applied to determine the overpotential (η) of the ORR in the buffered electrolyte solutions, by using the OCP potential (Eq. 4.2), or by applying the Nernst equation (Eq. 4.3). Here, $E_{cat/2}$ is the catalytic half-wave potential of the ORR by Cu-tmpa (Table 4.2), the standard reduction potential for the 4-electron reduction of O$_2$ in MeCN ($E_{O_2}^0$ = 1.21 V vs. Fc$^+$/Fc) was reported by Pegis et al,[27] and the standard reduction potential of H$^+$ in MeCN (E_{H+}^0= −0.028 V vs. Fc$^+$/Fc) was reported by Roberts et al.[21] As shown in Table 4.4, good agreement is achieved between both methods for

Table 4.4. Overview of the open-circuit potentials obtained in solutions containing HNEt₃⁺, HOAc, or their respective acid-conjugate base 1:1 mixture.

| Conditions		E_{OCP} (V vs. Fc⁺/Fc)	η_{OCP} (V)	η_{Nernst} (V)
HNEt₃PF₆ (50 mM)	No added water	−0.851		
	[H₂O] = 0.10 M	−0.825		
1:1 HNEt₃PF₆/NEt₃ (both 50 mM)	No added water	−1.148	0.77	0.78
	[H₂O] = 0.10 M	−1.132		
HOAc (20 mM)	No added water	−1.011		
	[H₂O] = 0.10 M	−1.017		
1:1 HOAc/NBu₄OAc (both 20 mM)	No added water	−1.207	0.80	0.59
	[H₂O] = 0.10 M	−1.178		

Conditions: NBu₄PF₆ (100 mM) in MeCN, 1 atm H₂, 293 K.

the HNEt₃⁺/NEt₃ system. However, a significant difference in results is obtained for HOAc/OAc⁺ as was expected based on the calculated $E^0_{H^+}$. While this was not further investigated, it could indicate a concentration effect in combination with influence of HOAc/OAc⁺ homoconjugation on the OCP value.

4.2.6. Acid concentration and time-dependence studies

Under non-catalytic conditions, a double redox event was observed in CVs of Cu-tmpa in the presence of HOAc. Similar behaviour was also observed for solutions containing HNEt₃PF₆ when an acid concentration below 50 mM was used. To investigate if the magnitude of the redox couples is dependent on the acid concentration in the electrolyte, CVs of electrolyte solutions containing 0.3 mM Cu-tmpa and acid in a range
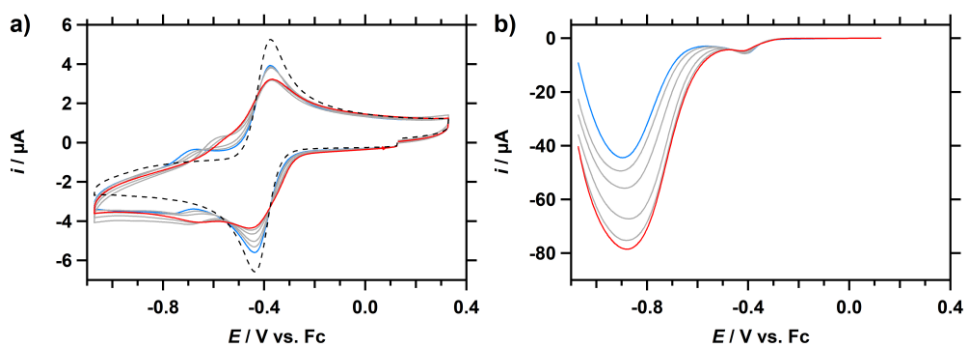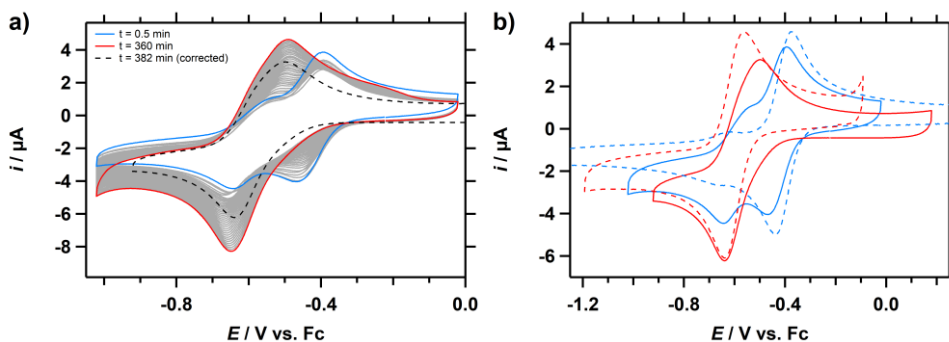

Figure 4.7. (a) CVs of Cu-tmpa (0.3 mM) in the presence of 1 atm Ar for different concentrations of HOAc, ranging from 5 mM (blue trace) to 100 mM (red trace), including a CV in the absence of acid (dashed trace). **(b)** Background-corrected LSVs of the ORR catalysed by Cu-tmpa over the same range of HOAc concentrations. Conditions: NBu₄PF₆ (100 mM) in MeCN, 100 mV s⁻¹, 293 K.
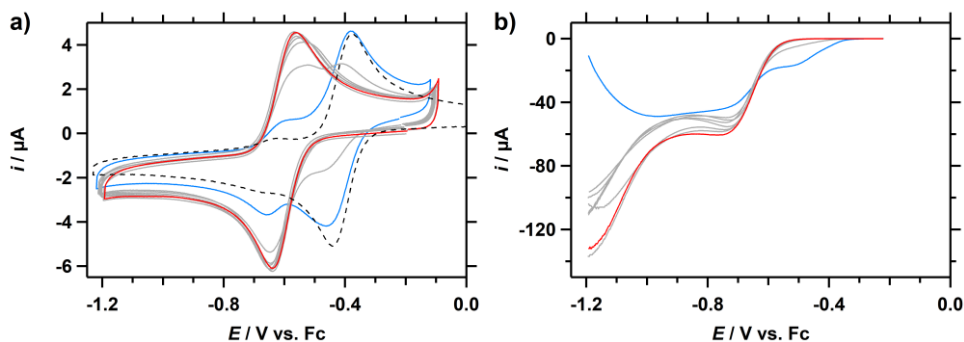
Figure 4.8. (a) CVs of Cu-tmpa (0.3 mM) in the presence of 1 atm Ar for different concentrations of HNEt$_3^+$, ranging from 10 mM (blue trace) to 100 mM (red trace), including a CV in the absence of acid (dashed trace). **(b)** Background-corrected LSV of the ORR by Cu-tmpa over the same range of HNEt$_3^+$ concentrations. Conditions: NBu$_4$PF$_6$ (100 mM) in MeCN, 100 mV s^{-1}, 293 K.

of concentrations between 5 and 100 mM were recorded, for both 1 atm Ar and O$_2$ (Figure 4.7). The main redox couple at −0.4 V shows a decreasing redox current with increasing acid concentration. At the same time, the second redox event becomes more pronounced yet also moves from −0.7 V to −0.6 V. The addition of the first 5 mM HOAc already results in a clear decrease of the oxidative and reductive current of the main redox couple and the appearance of the smaller second smaller redox couple mentioned before. Further increase of acid concentration does not seem to result in a linear decrease of the redox current. The effect of acid concentration is more pronounced for the ORR activity, as shown in Figure 4.7b. Here, the catalytic current increases linearly with the increased concentration (Figure C.4). However, one has to consider that this may be merely an effect of the proton concentration on catalysis, and not specifically on the concentration of catalytic species that can be associated with the increasing current response from the second redox couple (see Appendix C.4).

The same approach was taken to study the effect of the concentration of HNEt$_3$PF$_6$ on the redox chemistry and the catalytic ORR activity of Cu-tmpa. The resulting CVs over a range of acid concentration between 5 and 100 mM are shown in Figure 4.8. While the previously mentioned redox couple at −0.61 V is present at acid concentrations higher than 20 mM, at lower concentrations the most prominent redox couple of Cu-tmpa has the same redox potential as that of the complex in the absence of acid. However, several repeated CV measurements of Cu-tmpa in an electrolyte solution containing 50 mM HNEt$_3$PF$_6$ showed small fluctuations in the position and magnitude of the redox couple. This was initially thought to be caused by different water content in the solutions that were used in these experiments, but upon further investigation a time-based element was identified as a probable cause. To confirm this, every 5 minutes a CV was measured of an electrolyte solution containing 0.3 mM Cu-

Figure 4.9. (a) CVs of Cu-tmpa (0.3 mM) in the presence of 50 mM HNEt$_3$PF$_6$ under 1 atm Ar, measured at 5 min time intervals after addition of the acid **(b)** A comparison of CVs of 0.3 mM Cu-tmpa in the absence of acid (dashed blue trace), at t = 0.5 min after addition of 50 mM HNEt$_3^+$ (blue trace), at t = 382 min after addition of 50 mM HNEt$_3^+$ (red trace), and in a solution containing 100 mM HNEt$_3^+$ (dashed red trace). Conditions: NBu$_4$PF$_6$ (100 mM) in MeCN, 100 mV s^{-1}, 293 K.

tmpa and 50 mM HNEt$_3$PF$_6$ under 1 atm of Ar. The resulting CVs are shown in Figure 4.9a. Over the course of 6 hours, a chemical conversion took place between two different redox-active compounds, which were previously observed in the concentration dependence results. A comparison of the first (*t* = 0.5 min) and last (*t* = 382 min) CVs with the CVs obtained without acid and with 100 mM HNEt$_3$PF$_6$ shows that almost full conversion took place of the species with the less negative redox potential into the species with the more negative redox potential (Figure 4.9b). However, an additional shoulder is still present on both the reduction and oxidation domain indicates an equilibrium between the two species. Further analysis of the data (Appendix C.7) confirmed a species distribution ratio of 0.8 to 0.2. The combination of the HNEt$_3^+$ concentration dependence and the establishment of an equilibrium over time, indicates that protonation of the complex plays a role. By monitoring the species distribution as a function of time, the reaction order of this chemical conversion was determined. A plot of the natural logarithm of the species concentration vs. time (Figure C.9d) revealed that during the first 3 hours of the reaction it is governed by a first-order rate law. The resulting reaction rate was determined to be 8.27×10^{-5} s^{-1}, with a half-life of 140 minutes.

In addition to the electrochemical measurements, a solution with the same composition was monitored separately using UV-vis spectroscopy. Upon addition of HNEt$_3$PF$_6$ (50 mM), the absorption band corresponding to the characteristic Cu^{II} d–d transition is blue-shifted by 25 nm (Figure C.10). Over the course of 6 hours, a UV-vis spectrum was recorded every 5 minutes. However, the only change in the UV-vis spectrum over this period was a slight increase in the broad band around 300 nm, as
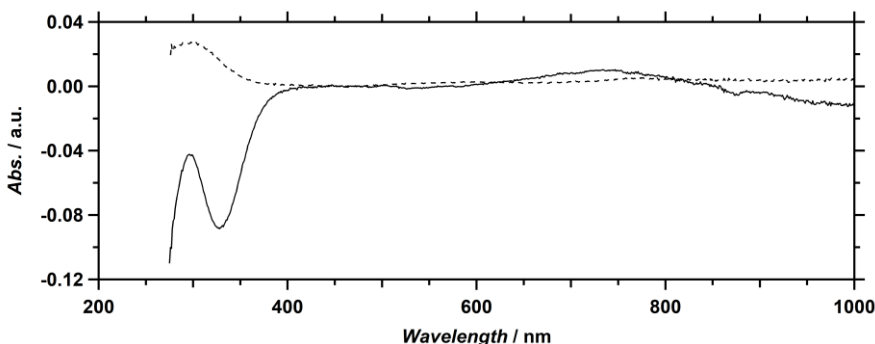
Figure 4.10. Difference spectrum after addition of HNEt$_3$PF$_6$ (black trace) to the electrolyte solution containing 0.3 mM Cu-tmpa and 100 mM NBu$_4$PF$_6$ in MeCN, and between the start at t = 0 min, and the end at t = 360 min (dashed trace).

shown in the difference spectrum of the UV-vis absorbance spectra at the start and end of the experiment (Figure 4.10).

4.2.7. Catalyst concentration dependence

To get more insight into the catalytic mechanism for the ORR by Cu-tmpa in MeCN, the relationship between the catalytic current and the catalyst concentration was investigated in the presence of HOAc and HNEt$_3^+$. CVs were measured in the presence of 1 atm of O$_2$ over a range of Cu-tmpa concentrations (10–300 µM). After a background correction was applied to filter out the catalytic activity caused by the GC electrode itself, a linear first-order relationship between the catalytic current and the catalyst concentration was observed, both for HNEt$_3$PF$_6$ and HOAc (Figure 4.11). The different acid concentrations, 50 mM HNEt$_3$PF$_6$ and 100 mM HOAc, result in the same peak catalytic currents, indicating that the acid concentration does not have a significant current-limiting effect on the catalysis under these conditions. Additionally, it shows that the ORR is not limited in O$_2$ at a catalyst concentration of 0.3 mM, as good linearity of i_{cat} is maintained in this higher catalyst concentration range.

4.2.8. Quantification of catalyst performance

To compare the electrocatalytic performance of Cu-tmpa for ORR in MeCN under different conditions, the observed catalytic rate constant k_{obs} (or turnover frequency; TOF) was determined from the catalytic current enhancement by applying equation 4.4.[28] The current enhancement was determined using the i_{cat} obtained over a range of catalyst concentrations (Figure 4.11), while i_p was calculated based on the diffusion coefficient of Cu-tmpa in the absence of any acid, using the Randles-Sevcik equation. Scan-rate dependence studies to obtain the diffusion coefficient in the presence of
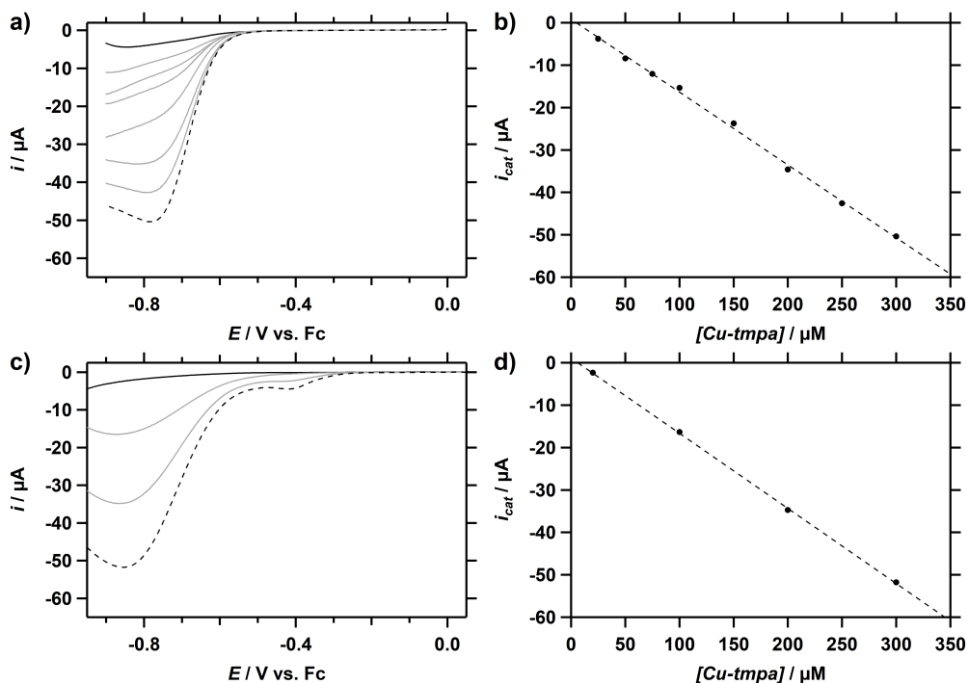
Figure 4.11. (a) Background-corrected LSVs of the catalytic ORR by Cu-tmpa in the presence of HNEt₃PF₆ (50 mM) under 1 atm O₂, for catalyst concentrations ranging from 25 (black) to 300 (dashed) μM. **(b)** Peak catalytic current i_{cat} at −0.78 V vs. Fc. **(c)** Background-corrected LSV of the catalytic ORR by Cu-tmpa in the presence of HOAc (100 mM) under 1 atm O₂, for catalyst concentrations ranging from 20 to 300 μM. **(d)** Peak catalytic current i_{cat} at −0.85 V vs. Fc. Conditions: NBu₄PF₆ (100 mM) in MeCN, 100 mV s⁻¹, 293 K.

different acids and acid-conjugate base mixtures revealed that often two different redox couples were present (Appendix C.1), whose distribution are also both concentration and time-dependent (see Section 4.2.6). This prevented accurate determination of diffusion coefficients under these conditions. As this was not an issue in the absence of acid, the diffusion coefficient of Cu-tmpa in an MeCN solution without acid was used as an approximation to determine the i_p in the presence of acid. Applying Eq. 4.4 resulted in k_{obs} for the ORR by Cu-tmpa of 4.5 ± 0.4 s⁻¹ and 5.0 ± 0.3 s⁻¹ for solutions containing HNEt₃PF₆ (50 mM) or HOAc (100 mM), respectively.

$$\frac{i_{cat}}{i_p} = 2.24n\sqrt{\frac{RT}{Fv}k_{obs}} \tag{4.4}$$

As described in Section 4.2.7 and as evidenced by the low k_{obs}, catalysis is not limited by O₂ concentration in the presence of 0.3 mM Cu-tmpa, which allows for the determination of the k_{obs} from any CV that was measured at this concentration and thus does not require a catalyst concentration dependence series. Thus, k_{obs} were

Table 4.5. Overview of k_{obs} obtained for the ORR and HPRR by Cu-tmpa under different catalytic conditions. Determined directly from CV measurements at 0.3 mM catalyst concentration.

Proton source	$k_{obs,ORR}$ (s^{-1})	$k_{obs,HPRR}$ (s^{-1})	
HNEt$_3$PF$_6$	4.6	35.9[a]	11.3[b]
HNEt$_3$PF$_6$/NEt$_3$	2.7	37.8	2.5[c]
HOAc	5.6	42.9	
HOAc/OAcNBu$_4$	1.5	4.5	2.2[b]

*[a] The maximum catalytic current was used as i_{cat}, [b] i_{cat} values were determined at −0.80 V vs. Fc, [c] i_{cat} values were determined at −0.75 V vs. Fc. For the ORR a catalytic electron transfer number of n = 4 was used.*

determined for solutions containing either HNEt$_3^+$, HNEt$_3^+$/NEt$_3$, HOAc, or HOAc/OAc$^-$, using the same concentrations as were used for the determination of the E_{BH^+} (Section 4.2.5). This was done for both the ORR and HPRR catalysed by Cu-tmpa (0.3 mM). For this purpose, i_{cat} values were determined from background corrected LSVs (Figure C.3). The resulting k_{obs} are shown in Table 4.5. For the $k_{obs,ORR}$, the catalytic electron transfer number used was 4, as under all four conditions both O$_2$ and H$_2$O$_2$ reduction take place at the potential where the k_{obs} was determined (Figure C.4, Appendix C.3). The $k_{obs,ORR}$ for HNEt$_3^+$ and HOAc are in good agreement with the k_{obs} obtained at low catalyst concentration for these acids. For three of the four conditions, two different k_{obs} values are calculated for the HPRR, as multiple catalytic waves were observed in the CVs and LSVs. Under those conditions, two distinct catalytic waves were visible in the LSV, and the smallest k_{obs} value corresponds to the catalytic current of first, smaller reduction wave, while the larger value corresponds to the maximum catalytic current, which takes place at more negative potentials. Compared to the rate constants observed in aqueous solution, the rate constants obtained in MeCN are several orders of magnitude lower, particularly for the ORR. This is in line with the very low equilibrium constant of formation for [Cu^{II}(O$_2^{\bullet-}$)(tmpa)]$^+$ that was observed in propionitrile (EtCN).[3]

4.3. Discussion

4.3.1. The redox behaviour of Cu-tmpa in the absence of acids

The reaction of Cu^I-tmpa with O$_2$ in the non-protic solvents EtCN, THF, and acetone has been well-studied.[2-3, 11] It has been shown that the initially formed Cu^I-tmpa complex reacts with O$_2$ to form an end-on Cu^{II} superoxide complex [Cu^{II}(O$_2^{\bullet-}$)(tmpa)]$^+$. However, nitriles are strongly coordinating ligands for Cu^I.[2, 29] In EtCN, the equilibrium constant of formation for [Cu^{II}(O$_2^{\bullet-}$)(tmpa)]$^+$ at room temperature is only 0.38 M^{-1} due to competition of O$_2$ with EtCN as a ligand for the Cu^I-tmpa complex (Scheme 4.2).[3] Additionally, the dimerization reaction of [Cu^{II}(O$_2^{\bullet-}$)(tmpa)]$^+$ with [Cu^I(tmpa)(EtCN)]$^+$ to form [{Cu^{II}(tmpa)}$_2$(μ–O$_2$)]$^{2+}$ occurs more slowly than the formation of the initial
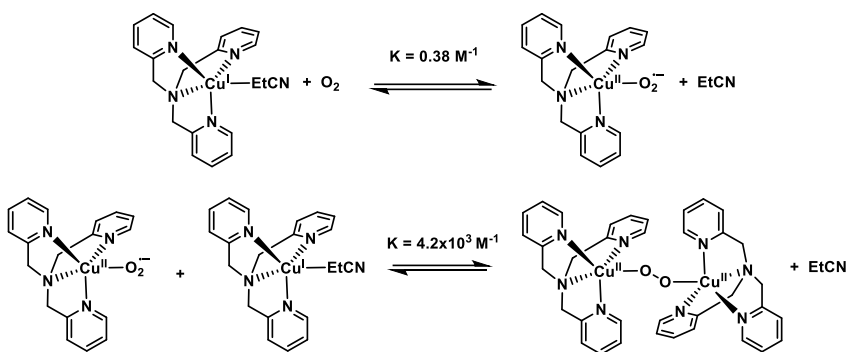
Scheme 4.2. Reaction scheme for the reaction of $[Cu^I(tmpa)(EtCN)]^+$ with O_2, with equilibrium constant of formation as reported in the literature.[2-3]

monomeric superoxide species, with a formation rate constant of 6.7×10^6 M^{-1} s^{-1} against 5.8×10^7 M^{-1} s^{-1} for the latter, but has a much higher equilibrium constant of formation of 4.2×10^3 M^{-1}, indicating better stability.

Our electrochemical measurements of Cu-tmpa in MeCN in the presence of dioxygen show a significant degree of irreversibility (Figures 4.1b and 4.1c). This poor electrochemical reversibility is characterized by an increased ΔE_p, a lowered oxidative current, and an irreversible reduction at a potential below -0.8 V vs. Fc$^+$/Fc. The lower oxidative current of the Cu$^{II/I}$ redox couple is partially the result of the above mentioned equilibrium constant of $[Cu^{II}(O_2^{\bullet-})(tmpa)]^+$, which is expected to be of a similar magnitude in MeCN. Due to the equilibrium between $[Cu^I(tmpa)(L)]^+$ and $[Cu^{II}(O_2^{\bullet-})(tmpa)]^+$ part of the Cu^I is sequestered as the superoxido species upon reacting with O_2, thus lowering the oxidation current of the Cu$^{II/I}$ redox couple. However, in the timeframe of the CV only a small or even negligible reduction in oxidative current would be expected due the very fast rates associated with this forward and reverse reactions (in Scheme 4.2), maintaining the equilibrium while the electrochemical oxidation of Cu^I takes place. Additionally, formation of the dimeric peroxido species may explain the increase in ΔE_p, due to lower reversibility of the redox chemistry caused by sequential electrochemical and chemical reactions. This would also contribute to the reduced redox current over multiple scans (Figure 4.1c), as over time some of the dimer may accumulate near the electrode. A complicating factor is the presence of trace amounts of water, and thus protons, in MeCN. For the experiments shown in Figure 4.1, 0.5 mM of H_2O was detected using Karl-Fisher titration following drying of the solvent, which is close to a 1:2 ratio of catalyst to water. A proton-coupled electron transfer (PCET) step from the initially formed superoxido species would result in the formation of the hydroperoxide complex $[Cu^{II}(OOH)(tmpa)]^+$. This species could react further, resulting in the formation of H_2O,

or even H_2O_2 following a simple protonation. Alternatively, the dimer, which has been shown to be able to catalyse the ORR in acetone using Fc as a reductant, can be further reduced to a Cu^I–OO–Cu^{II} species. The irreversible reduction that is observed below -0.8 V can be the result of either of these proposed steps. While the magnitude of the reductive current is similar to that of the one-electron reduction of Cu^{II}-tmpa to Cu^I-tmpa, it cannot be excluded that this is actually a small catalytic wave resulting from the presence of trace amounts of water.

4.3.2. Redox behaviour of Cu-tmpa in the presence of different acids

For several of the studied electrochemical conditions, multiple redox couples were observed during CV measurements of Cu-tmpa. Reproducibility of the redox couple of Cu-tmpa in acetonitrile in the presence of $HNEt_3^+$ (50 mM) appeared to be poor, as two redox couples with varying relative intensity were observed in several experiments. Initially, it was assumed that perhaps variable water content in the electrolyte solution was the cause of the varying ratios of the two visible redox couples. However, the ultimate cause appeared to be a time-dependent chemical conversion that takes place in the electrolyte solution. Indeed, most experiments that were performed under these conditions show a different distribution of the two distinct redox couples, which seems to be an effect of the difference in time between preparation of the solution and the actual electrochemical measurement. The redox couple at the less negative potential overlaps to a large degree with the redox couple of Cu-tmpa in NBu_4PF_6, which is assigned to $[Cu(tmpa)(CH_3CN)]^{2+}$. This is particularly clear at lower concentrations of $HNEt_3^+$ concentrations (Figure 4.8a).

We observed both a time-dependent conversion and a concentration-dependent effect, where higher initial $HNEt_3^+$ concentrations resulted in an increased redox current of the species with the more negative $E_{1/2}$, which indicates that protonation of the ligand plays a role. This is also in line with the observed stability of the ratio between the two redox couples over time in the buffered electrolyte solution containing $HNEt_3^+/NEt_3$ in a 1:1 ratio, where no new equilibrium is established. UV-Vis absorption spectra of a solution containing Cu-tmpa upon addition of $HNEt_3^+$ (or $HNEt_3^+/NEt_3$) showed a small blueshift of the d-d transition band by 25 nm, which may indicate protonation of coordinated nitrogen atoms but this is not conclusive. However, no significant changes in the absorption where observed over time, contrary to the clear chemical conversion observed during the CV measurements. Several considerations can be made on the nature of the redox-active species associated with the redox couple at more negative potentials. The possibility of coordination of the NEt_3 conjugate base can largely be discounted as nitriles such a MeCN are much better ligands for Cu^{II} and Cu^I species. Protonation of one or multiple nitrogen atoms in the ligand could result in

the dissociation of one of the N-donors. Dissociation of one of the pyridine arms of the ligand caused by the protonation of the pyridine seems unlikely, as NEt$_3$ (conjugate acid pK_a = 18.8) is also a stronger base than pyridine (conjugate acid pK_a = 12.5) in MeCN.[30] This would have resulted in an increase of the redox potential of the species, as opposed to the observed decrease, as observed for copper complexes containing the bis(2-pyridylmethyl)amine ligand.[31-32] Additionally, it has been shown the tertiary aliphatic amine in the free tmpa ligand is less basic than the pyridine N-atom, contrary to the generally expected higher basicity of tertiary aliphatic amines.[33-35] While selective protonation of the tertiary amine of tmpa has been observed in a strained environment,[36-37] it is not known whether the same would occur when coordinated to a copper ion. For a wide range of copper complexes with multidentate ligands, it has been shown that the Cu$^{II/I}$ redox potential is mainly influenced by the stability of the Cu^{II} species, while the corresponding Cu^{I} species show near uniform stability.[38-39] How protonation of the tmpa ligand would result in a more stable Cu^{II} complex, with better orbital overlap or increased electron density on the copper centre, is unclear and the exact nature of the species can not be predicted based on the available data.

The Cu$^{II/I}$ redox couple of Cu-tmpa in the electrolyte solution containing HOAc is located at the same potential (−0.40 V) as in the acid-free electrolyte solution. This would indicate that no chemical conversion takes place upon addition of low (20 mM) amounts of acid and [Cu(tmpa)(CH$_3$CN)]$^{2+}$ is still the main species in solution. As the HOAc concentration is increased from 20 to 100 mM, the current of the redox couple decreases only slightly and a second smaller redox couple is observed at a more negative potential. However, HOAc is a weaker acid than HNEt$_3^+$ (Table 4.1) and ligand protonation is therefore unlikely to play a role. The CVs of Cu-tmpa in the buffered acid-conjugate base HOAc/OAc$^-$ solution shows a single well-defined redox couple at a more negative potential (−0.73 V), while UV-vis absorption spectra under the same conditions show the presence of a LMCT band and blueshifted d-d band, which indicates the coordination of anionic acetate to the copper centre (Appendix C.9). Acetate is a good ligand for copper and is not readily replaced by MeCN under standard conditions.[40-42] Indeed, it has been previously shown that the addition of trifluoroacetic acid to [Cu^{II}(tmpa)]$^{2+}$ in acetone resulted in the formation of [Cu^{II}(tmpa)(CF$_3$COO$^-$)]$^+$, causing a −300 mV shift in the redox potential due to the increased electron density on the Cu centre.[14] Thus, the redox couple at −0.73 V is associated with the compound [Cu^{II}(OAc)(tmpa)]$^+$. In contrast, for unbuffered solutions containing HOAc, the concentration of available OAc$^-$ is not high enough to replace MeCN in the coordination sphere, which would explain why the intensity of the second redox event is low.

4.3.3. Catalytic performance of Cu-tmpa for the ORR in MeCN

The electrocatalytic reduction of O_2 by Cu-tmpa in MeCN is significantly slower than in aqueous solution, despite oxygen having a six times higher solubility in MeCN than in water at 1 atm O_2 at room temperature.[17] The k_{obs} for ORR that were calculated based on the current enhancement in MeCN (1.5-5.6 s^{-1}) are a factor 10^5 lower than the TOF in a neutral aqueous solution (1.5×10^5 s^{-1}, Chapter 2). The overpotential (defined by $E_{cat/2}$) for the ORR with Cu-tmpa are lower in the buffered MeCN solutions (below 0.8 V) than in neutral aqueous solution (0.92 V), as shown in Table 4.4. For both HOAc and $HNEt_3^+$ a linear relationship between the catalytic current and the Cu-tmpa concentration was observed, indicating a first-order catalytic reaction in catalyst, as was also observed in a neutral aqueous solution. Interestingly, a first-order dependence of the catalytic current on the acid concentration was found with HOAc in MeCN, while in the case of $HNEt_3^+$ the catalytic rates were independent of the acid concentration, as shown in Appendix C.4. These findings indicate that the rate-determining step of the catalytic reaction in the presence of HOAc does not only involve the catalyst, but also the acid (or H^+) species. For $HNEt_3^+$, the changing catalytic behaviour can be directly linked to the concentration-induced change of the redox active species. Once this interconversion is fully completed, a further increase in acid concentration does not lead to an appreciable increase in catalytic current (Figure 4.8). Thus, different rate laws govern the ORR by Cu-tmpa in the presence of HOAc and $HNEt_3^+$.

   With these observations, the catalytic mechanism for the ORR in MeCN in the presence of AcOH shows strong similarities to the mechanism observed in aqueous solution, as shown in Scheme 4.1, with some small modifications. As stated, the rate-determining step involves a single Cu centre, but also involves a protonation step, likely the H^+/e^- PCET step from $[Cu^{II}(O_2{}^{\bullet-})(tmpa)]^+$ to $[Cu^{II}(OOH)(tmpa)]^+$. Despite the expected unfavourable thermodynamic equilibrium for the binding of O_2 to $[Cu^I(MeCN)(tmpa)]^+$, the kinetic rate constant of formation (k_1) is very high (5.8×10^7 M^{-1} s^{-1} in EtCN).[3] When a rapid equilibrium, like the reversible binding of O_2 to Cu^I, is followed by a slow step, the overall observed rate constant is a function of both the equilibrium constant and the rate constant of the subsequent slower reaction step, in accordance with the pre-equilibrium approximation.[43] Thus, while the PCET step would be the rate-determining step, the binding of O_2 is still involved in the overall rate constant of the ORR catalysed by Cu-tmpa in MeCN.

4.3.4. Catalytic performance of Cu-tmpa towards the HPRR in MeCN

Like the reduction of O_2, the reduction of H_2O_2 in MeCN (k_{obs} = 2.2-43 s^{-1}) is slower than in neutral aqueous solution (k_{obs} = 4.8×10^3 s^{-1}, Chapter 3), but only by a factor 100 to 1000. Additionally, in MeCN, the HPRR is generally faster under these conditions than

the ORR, whereas in water the opposite is the case. This holds true both in the presence and absence of base. This behaviour seems to point at Cu^{II}-OOH being more readily formed from the reaction of Cu^I-tmpa with H_2O_2 than with O_2 in MeCN, perhaps mediated by the presence of 30 mM of H_2O in the solution. Indeed, in the presence of a base and H_2O_2 $[Cu^{II}(OOH)(tmpa)]^+$ is spontaneously formed from $[Cu^{II}(tmpa)(L)]^{2+}$ (Appendix C.9).

A comparison of the maximum HPRR k_{obs} under different conditions shows similar values in solutions containing $HNEt_3^+$, $HNEt_3^+/NEt_3$, or HOAc (Table 4.5). However, the k_{obs} (of the first and second catalytic wave) is at least one order of magnitude lower in the presence of the acid-conjugate base pair $HOAc/OAc^-$ than for the other conditions. This behaviour validates the previously discussed formation of $[Cu^{II}(tmpa)(OAc)]^+$ when $HOAc/OAc^-$ is present in solution. Formation of this species results in a lowered catalytic activity for the HPRR caused by the stronger coordination of acetate compared to MeCN, in essence blocking the active site of the catalyst for H_2O_2 binding. While spontaneous formation of the Cu^{II}-OOH species was detected under non-catalytic conditions in MeCN, the UV-vis absorbance around 400 nm associated with this species was almost three times lower in the presence of $HOAc/OAc^-$ versus $HNEt_3^+/NEt_3$. Furthermore, the absorption band at 400 nm was also only visible 22 hours after addition of H_2O_2 to the solution containing $HOAc/OAc^-$, as opposed to the immediate appearance of this band in the presence of $HNEt_3^+/NEt_3$. This again shows that the formation of the Cu^{II}-OOH species is slower for $[Cu^{II}(OAc)(tmpa)]^+$. However, the effect of the strong homoconjugation of acetic acid cannot be excluded in this discussion, as the lowered proton availability could also explain part of the lowered catalytic activity of Cu-tmpa towards HPRR in presence of HOAc. The second catalytic wave in the presence of $HOAc/OAc^-$, might be the result of H_2O acting as the proton source, which would require a higher driving force, and thus a higher overpotential.

4.4. Conclusion

The influence was investigated of different acids and acid-conjugate base mixtures on the electrocatalytic O_2 and H_2O_2 reduction by Cu-tmpa in acetonitrile. It was shown that the use of proton donors with a lower pK_a resulted in destabilisation of the Cu-tmpa compound. This was apparent from the lack of reversible redox couples in the presence of HTFA and $HDMF^+$, something which was also observed for Cu-tmpa at lower pH (<4) in aqueous electrolyte solution. In all cases, higher catalytic k_{obs} were observed for the ORR in the unbuffered electrolyte solutions containing only the acid species. Coordination of acetate is the likely cause of the reduced catalytic activity in solution containing $HOAc/OAc^-$, which is harder to replace in the coordination sphere, thus inhibiting catalysis. This is even more obvious for the HPRR. The reduction of the

catalytic activity is smaller in the presence of triethylamine, and is likely the result of the established equilibrium between $[Cu(tmpa)(CH_3CN)]^{2+}$ and the as of yet unidentified species with a more negative redox potential. In contrast to the catalytic behaviour of Cu-tmpa in neutral aqueous solutions, higher TOFs were observed for the HPRR than for the ORR in MeCN under each of the different conditions that were investigated. This points to a more positive formation constant for the LCu^{II}-OOH complex than for LCu^{II}-OO$^{\bullet-}$ under these conditions. As was observed under aqueous conditions, the catalytic rate showed a first-order dependence in catalyst concentration, confirming a mononuclear catalytic mechanism for Cu-tmpa under electrochemical conditions. Interestingly, the k_{obs} for the ORR shows a first-order dependence on the acid concentration in the electrolyte solution containing HOAc. These results confirm that in the presence of HOAc the catalytic mechanism for ORR in MeCN is largely the same as in water, although the rate-determining step in MeCN is the PCET step from $[Cu^{II}(O_2^{\bullet-})(tmpa)]^+$ to form $[Cu^{II}(OOH)(tmpa)]^+$.

4.5.   Experimental

4.5.1.   General

Tetrabutylammonium hexafluoridophosphate (≥99.0%, for electrochemical analysis) tetrabutylammonium hydroxide (1.1 M in MeOH), ammonium hexafluoridophosphate, and acetic acid (99.99% trace metal basis) were obtained from Sigma-Aldrich. Triethylamine (≥99.8%, for LC-MS) was obtained from VWR and ferrocene (>98%) was obtained from Fluka. The copper complex $[Cu(tmpa)(MeCN)](OTf)_2$ was synthesized as described in Chapter 2. Acetonitrile (99.9%, HPLC grade, BioSolve) was further dried over activated molecular sieves for 4 days. Molecular sieves (3 Å, Sigma Aldrich) were first rinsed with acetonitrile to remove impurities and loose solid particles, and activated by drying at 140 °C in a vacuum oven at <10 mbar for 2 days.

4.5.2.   Electrochemical measurements

Autolab PGSTAT 12, 204, and 128N potentiostats in combination with Autolab NOVA 2 software were used for all measurements. Electrochemical measurements were performed in a custom-build 10 mL glass single-compartment cell with a three-electrode setup, or a single compartment cell based on single-use 20 mL glass vials, allowing for a four-electrode setup, in the same approach as reported by Roberts and Bullock.[21]

The 10 mL single-compartment cell used during the electrochemical measurements was regularly cleaned to remove impurities by overnight submersion in an aqueous 0.5 M H_2SO_4 solution containing 1 mg/mL (6.3 mM) $KMnO_4$, followed by removal of excess

KMnO$_4$ and MnO$_2$ from the glassware with diluted H$_2$SO$_4$ and H$_2$O$_2$. Finally, the glassware was rinsed five times and subsequently boiled two times in Milli-Q water. Prior to each experiment all glassware was boiled once in Milli-Q water and oven-dried overnight at 120 °C. A PEEK encapsulated glassy carbon (A = 0.0707 cm^2, Metrohm) was used as the working electrode in a submerged setup. Before every experiment, the GC electrodes were manually polished for 5 mins each with 1.0, 0.3, and 0.05 µm alumina suspensions on Buehler cloth polishing pads, followed by sonication in MeCN for 10 minutes. A gold wire was used as the counter electrode and was flame annealed and rinsed with Milli-Q water before each experiment. A double-junction reference electrode (Methrohm) was used, either used as a 0.3 M Ag/AgCl reference, or as a Ag/AgNO$_3$ reference. For the Ag/AgNO$_3$ solution, the inner junction was filled with 10 mM AgNO$_3$ in MeCN, while the outer junction was filled with 100 mM NBu$_4$PF$_6$ in MeCN. The potential and stability of the Ag/AgNO$_3$ reference electrode was carefully monitored, and the solution was refreshed when necessary (Appendix C.6). All measurements were referenced to the Fc$^+$/Fc redox couple.

All gasses used during electrochemical measurements, O$_2$ (5.0 grade), and argon (5.0 grade), were supplied by Linde. Oxygen-free electrolyte solutions were prepared by sparging the solution for 30 minutes with argon, after which a 1 atm argon atmosphere was maintained. Oxygen-saturated electrolyte solutions were obtained by sparging the cell for 20 minutes with O$_2$, after which a 1 atm O$_2$ atmosphere was maintained. All gases were pre-saturated with MeCN through a pre-bubbler before being passed through the electrochemical cell.

4.5.3.   OCP measurements

A Pt wire was used for the determination of the open circuit potential (OCP). The Pt wire was flame-annealed and subsequently electropolished in a 0.1 M H$_2$SO$_4$ aqueous solution for 25 to 50 cycles at 500 mV s^{-1} between −0.05 and 1.9 V vs. RHE before every experiment. For every different electrolyte mixture, a new 20 mL glass vial was used thoroughly rinsed with MeCN and dried in the oven. The hydrogen and argon gas were pre-saturated with solvent by bubbling through acetonitrile, which was dried over activated molecular sieves (3Å). 5 mL of the desired MeCN electrolyte solution, containing both NBu$_4$PF$_6$ (100 mM) and the desired acid-conjugated base mixture, was added to the glass vial, followed by bubbling with a MeCN saturated flow of H$_2$ for 2-5 minutes. The OCP was measured by the Pt wire electrode over a period of 60 seconds, while vigorously bubbling the solution with H$_2$. This was repeated until a stable OCP value was found. Subsequently Fc was added to the solution, and under a H$_2$ flow over the solution, a CV was measured with a GC electrode to obtain the $E_{1/2}$ of Fc$^+$/Fc.

4.5.4.   Catalyst concentration dependence studies

For the determination of the catalytic current i_{cat} as a function of Cu-tmpa concentration, the GC electrode was polished with 0.05 µnm alumina suspension for 5 minutes, rinsed with MilliQ and subsequently sonicated in MeCN for 10 minutes for every different catalyst concentration. Upon addition of aliquots of Cu-tmpa (10 mM in MeCN), the electrolyte solution was mixed thoroughly in both cell compartments and the solution was saturated with oxygen by bubbling the solution for 10 minutes with O_2 pre-saturated with MeCN. After the last measurement, Fc was added to the solution and the $E_{1/2}$ of Fc^+/Fc was measured. Additionally, a blank CV was measured of the GC electrode in an oxygen-saturated electrolyte solution in the absence of Cu-tmpa. The catalytic currents from CV measurements obtained in the presence of Cu-tmpa were corrected using this blank measurement, giving the catalytic current without any contribution from the GC electrode.

4.5.5.   Acid concentration dependence studies

For the determination of the catalytic current i_{cat} as a function of acid concentration, the GC electrode was polished with 0.05 µnm alumina suspension for 5 minutes, rinsed with MilliQ and subsequently sonicated in MeCN for 10 minutes for each different catalyst concentration. Cu-tmpa (0.3 mM) and Fc were dissolved in the electrolyte solution (100 mM NBu_4PF_6) and transferred to the electrochemical cell. Of this solution, 1 mL was used to dissolve the solid $HNEt_3PF_6$, kept under argon, which was transferred back into the electrochemical cell to reach the required acid concentration. The solution was thoroughly mixed and subsequently saturated with argon by bubbling for 10 minutes with 1 atm Ar pre-saturated with MeCN. A CV was measured to obtain the redox couple of Cu-tmpa, after which the solution was saturated with oxygen by bubbling for 10 minutes with O_2 pre-saturated with MeCN. After a CV was measured to obtain the catalytic current, a CV was measured in a potential window between 0.1 to 0.8 V vs. Ag/AgCl to obtain the $E_{1/2}$ of Fc. This process was repeated for all the different acid concentrations. The same methodology was followed to measure blank CVs of the GC electrode in the absence of Cu-tmpa.

4.5.6.   Synthesis

4.5.6.1.   *Synthesis of triethylammonium hexafluoridophosphate (HNEt₃PF₆)*

NH_4PF_6 (6.52 g, 40 mml) was suspended in toluene (40 mL), followed by the addition of triethylamine (5.58 mL, 40 mmol). The mixture was stirred and refluxed for 2 hours, after which the solution was allowed to cool down. The precipitate was filtered by vacuum filtration and washed with toluene (4x 15 mL). After drying in air, the product

was obtained as a white crystalline solid. The NMR is in good agreement with those reported in the literature.[44] Yield: 99% (9.78 g, 39.6 mmol). ^{1}H NMR (400 MHz, DMSO-d6) δ 3.37 (br), 3.09 (q, J = 7.3 Hz, 6H), 1.17 (t, J = 7.3 Hz, 9H).

4.5.6.2.   *Synthesis of tetrabutylammonium acetate*

Tetrabutylammonium acetate was prepared in methanol (MeOH) as described in literature.[45-47] Acetic acid (630 μL, 11 mmol) was dissolved in MeOH (10 mL). NBu$_4$OH in MeOH (7.9 ml, 11 mmol) was added. The reaction was stirred over night at room temperature. The solvents were evaporated at reduced pressure (65 °C) and the resulting product was liquid at high temperatures (65 °C). When cooled to room temperature the product crystallizes. The solid was washed twice with hexane (10 mL). Recrystallisation was done by dissolving the product in toluene (5 mL) and was crashed out by adding an excess amount of hexane. The hexane was removed by decantation and additional hexane was added twice leaving the product on the bottom of the round bottom flask. The product was dissolved in toluene (10 mL). The toluene was removed at reduced pressure. The product (quantitative yield) was further dried at low vacuum (<1 mbar) overnight. ^{1}H NMR (300 MHz, Chloroform-d) δ 3.38 – 3.29 (m, 9H), 1.94 (s, 3H), 1.72 – 1.57 (m, 9H), 1.42 (h, J = 7.3 Hz, 9H), 0.99 (t, J = 7.3 Hz, 12H).

4.5.6.3.   *Synthesis of dimethylformamidium trifluoromethanesulfonate ((HDMF)OTf)*

Dimethylformamidium trifluoromethanesulfonate ([HDMF]OTf) was synthesized following the reported procedure. Dimethylformamide (DMF) (0.87 mL, 11.3 mmol) was added to dichloromethane (DCM) (30 mL) using a glass pipette. The mixture was stirred and triflic acid (HOTf) (1.0 mL, 11.3 mmol) was added dropwise to the mixture using a glass pipette. The mixture was stirred for 10 minutes for the reactants to react in a one-step protonation. After 10 minutes a clear solution was obtained and the solvents were evaporated: first DCM was removed (40 °C, 700 mbar). After DCM was evaporated the temperature was increased and the pressure lowered (70 °C, 10mbar). After 30 minutes about 1-2 mL of clear solution was left in the round-bottom flask. The solution crystalized into a white crystalline solid after cooling to room temperature at normal pressure. The crystalline solid was dried overnight at low vacuum, yielding a white crystalline solid (2.5 g, quantitative yield). The crystals were stored under inert atmosphere. ^{1}H NMR (400 MHz, Chloroform-d) δ 8.89 (br s, 1H), 8.49 (s, 1H), 3.32 (s, 3H), 3.16 (s, 3H).

4.6.   References

[1]   M. Langerman, D. G. H. Hetterscheid, *Angew. Chem. Int. Ed.* **2019**, *58*, 12974-12978.

[2]   H. C. Fry, D. V. Scaltrito, K. D. Karlin, G. J. Meyer, *J. Am. Chem. Soc.* **2003**, *125*, 11866-11871.

[3]   C. X. Zhang, S. Kaderli, M. Costas, E.-i. Kim, Y.-M. Neuhold, K. D. Karlin, A. D. Zuberbühler, *Inorg. Chem.*

2003, *42*, 1807-1824.

[4]   Y. Lee, et al., *Inorg. Chem.* **2009**, *48*, 11297-11309.

[5]   T. Fujii, A. Naito, S. Yamaguchi, A. Wada, Y. Funahashi, K. Jitsukawa, S. Nagatomo, T. Kitagawa, H. Masuda, *Chem. Commun.* **2003**, 2700-2701.

[6]   H. R. Lucas, G. J. Meyer, K. D. Karlin, *J. Am. Chem. Soc.* **2010**, *132*, 12927-12940.

[7]   M. J. Baldwin, P. K. Ross, J. E. Pate, Z. Tyeklar, K. D. Karlin, E. I. Solomon, *J. Am. Chem. Soc.* **1991**, *113*, 8671-8679.

[8]   L. M. Mirica, X. Ottenwaelder, T. D. P. Stack, *Chem. Rev.* **2004**, *104*, 1013-1046.

[9]   C. E. Elwell, N. L. Gagnon, B. D. Neisen, D. Dhar, A. D. Spaeth, G. M. Yee, W. B. Tolman, *Chem. Rev.* **2017**, *117*, 2059-2107.

[10]   S. Itoh, *Curr. Opin. Chem. Biol.* **2006**, *10*, 115-122.

[11]   S. Fukuzumi, H. Kotani, H. R. Lucas, K. Doi, T. Suenobu, R. L. Peterson, K. D. Karlin, *J. Am. Chem. Soc.* **2010**, *132*, 6874-6875.

[12]   L. Tahsini, H. Kotani, Y. M. Lee, J. Cho, W. Nam, K. D. Karlin, S. Fukuzumi, *Chem. Eur. J.* **2012**, *18*, 1084-1093.

[13]   S. Fukuzumi, L. Tahsini, Y.-M. Lee, K. Ohkubo, W. Nam, K. D. Karlin, *J. Am. Chem. Soc.* **2012**, *134*, 7025-7035.

[14]   S. Kakuda, R. L. Peterson, K. Ohkubo, K. D. Karlin, S. Fukuzumi, *J. Am. Chem. Soc.* **2013**, *135*, 6513-6522.

[15]   D. Das, Y.-M. Lee, K. Ohkubo, W. Nam, K. D. Karlin, S. Fukuzumi, *J. Am. Chem. Soc.* **2013**, *135*, 2825-2834.

[16]   N. Le Poul, et al., *J. Am. Chem. Soc.* **2009**, *131*, 17800-17807.

[17]   M. L. Pegis, C. F. Wise, D. J. Martin, J. M. Mayer, *Chem. Rev.* **2018**, *118*, 2340-2391.

[18]   M. König, J. Vaes, E. Klemm, D. Pant, *iScience* **2019**, *19*, 135-160.

[19]   S. Garg, M. Li, A. Z. Weber, L. Ge, L. Li, V. Rudolph, G. Wang, T. E. Rufford, *J. Mater. Chem. A* **2020**, *8*, 1511-1544.

[20]   L. Sun, V. Reddu, A. C. Fisher, X. Wang, *Energy Environ. Sci.* **2020**, *13*, 374-403.

[21]   J. A. S. Roberts, R. M. Bullock, *Inorg. Chem.* **2013**, *52*, 3823-3835.

[22]   M. L. Pegis, J. A. S. Roberts, D. J. Wasylenko, E. A. Mader, A. M. Appel, J. M. Mayer, *Inorg. Chem.* **2015**, *54*, 11883-11888.

[23]   I. M. Kolthoff, M. K. Chantooni, *J. Am. Chem. Soc.* **1963**, *85*, 426-430.

[24]   J. F. Coetzee, G. R. Padmanabhan, *J. Am. Chem. Soc.* **1965**, *87*, 5005-5010.

[25]   Z. Pawlak, G. Zundel, J. Fritsch, A. Wawrzynów, S. Kuna, M. Tusk, *Electrochim. Acta* **1984**, *29*, 391-395.

[26]   M. Asahi, S.-i. Yamazaki, S. Itoh, T. Ioroi, *Electrochim. Acta* **2016**, *211*, 193-198.

[27]   M. L. Pegis, B. A. McKeown, N. Kumar, K. Lang, D. J. Wasylenko, X. P. Zhang, S. Raugei, J. M. Mayer, *ACS Cent. Sci.* **2016**, *2*, 850-856.

[28]   R. M. Bullock, A. M. Appel, M. L. Helm, *Chem. Commun.* **2014**, *50*, 3125-3143.

[29]   F. H. Jardine, in *Advances in Inorganic Chemistry and Radiochemistry, Vol. 17* (Eds.: H. J. Eméleus, A. G. Sharpe), Academic Press, **1975**, pp. 115-163.

[30]   S. Tshepelevitsh, A. Kütt, M. Lõkov, I. Kaljurand, J. Saame, A. Heering, P. G. Plieger, R. Vianello, I. Leito, *Eur. J. Org. Chem.* **2019**, *2019*, 6735-6748.

[31]   A. Kunishita, J. D. Scanlon, H. Ishimaru, K. Honda, T. Ogura, M. Suzuki, C. J. Cramer, S. Itoh, *Inorg. Chem.* **2008**, *47*, 8222-8232.

[32]   M. Asahi, S.-i. Yamazaki, S. Itoh, T. Ioroi, *Dalton Trans.* **2014**, *43*, 10705-10709.

[33]   G. Anderegg, K. Popov, P. S. Pregosin, *Helv. Chim. Acta* **1986**, *69*, 329-332.

[34]   A. Hazell, J. McGinley, H. Toftlund, *Dalton Trans.* **1999**, 1271-1276.

[35]   G. Anderegg, E. Hubmann, N. G. Podder, F. Wenk, *Helv. Chim. Acta* **1977**, *60*, 123-140.

[36]   L. Zhiquan, H. Xie, S. E. Border, J. Gallucci, R. Z. Pavlović, J. D. Badjić, *J. Am. Chem. Soc.* **2018**, *140*, 11091-11100.

[37]   G. Qiu, C. Colomban, N. Vanthuyne, M. Giorgi, A. Martinez, *Chem. Commun.* **2019**, *55*, 14158-14161.

[38]   E. A. Ambundo, M.-V. Deydier, A. J. Grall, N. Aguera-Vega, L. T. Dressel, T. H. Cooper, M. J. Heeg, L. A. Ochrymowycz, D. B. Rorabacher, *Inorg. Chem.* **1999**, *38*, 4233-4242.

[39]   D. B. Rorabacher, *Chem. Rev.* **2004**, *104*, 651-698.

[40]   M. Vaidyanathan, R. Viswanathan, M. Palaniandavar, T. Balasubramanian, P. Prabhaharan, P. Muthiah, *Inorg. Chem.* **1998**, *37*, 6418-6427.

[41]   H. Adams, N. A. Bailey, C. O. R. de Barbarin, D. E. Fenton, Q.-Y. He, *J. Chem. Soc., Dalton Trans.* **1995**, 2323-

2331.

[42]   S. Meghdadi, M. Amirnasr, A. Amiri, Z. Musavizadeh Mobarakeh, Z. Azarkamanzad, *C. R. Chim.* **2014**, *17*, 477-483.

[43]   M. Rae, M. N. Berberan-Santos, *Chem. Phys.* **2002**, *280*, 283-293.

[44]   B. M. Trost, R. C. Livingston, *J. Am. Chem. Soc.* **2008**, *130*, 11970-11978.

[45]   S. E. Denmark, M. T. Burk, A. J. Hoover, *J. Am. Chem. Soc.* **2010**, *132*, 1232-1233.

[46]   P. Hamankiewicz, J. M. Granda, J. Jurczak, *Tetrahedron Lett.* **2013**, *54*, 5608-5611.

[47]   H. Nagae, R. Aoki, S.-n. Akutagawa, J. Kleemann, R. Tagawa, T. Schindler, G. Choi, T. P. Spaniol, H. Tsurugi, J. Okuda, K. Mashima, *Angew. Chem. Int. Ed.* **2018**, *57*, 2492-2496.